coatings

MDPI

Article

Investigation on Solar Absorption and Thermal Emittance of Al Films Deposited by Magnetron Sputtering

Jinxin Gu [1], Xin Zhao [2,3,*], Feifei Ren [2], Hang Wei [2], Shuhui Liang [1], Chenchen Geng [2], Huan Guan [2], Xiang Zhang [2], Shuliang Dou [2,*] and Yao Li [2,*]

1 School of Chemical Engineering and Technology, Harbin Institute of Technology, Harbin 150001, China; gujinxin1995@163.com (J.G.); 20B925024@stu.hit.edu.cn (S.L.)
2 Center for Composite Materials and Structure, Harbin Institute of Technology, Harbin 150001, China; rff016813@163.com (F.R.); 19b918072@stu.hit.edu.cn (H.W.); gengchenHIT@163.com (C.G.); 20B918080@stu.hit.edu.cn (H.G.); zhangxhit@hit.edu.cn (X.Z.)
3 Beijing Key Laboratory of Space Thermal Control Technology, Beijing Institute of Spacecraft System Engineering, China Academy of Space Technology, Beijing 100094, China
* Correspondence: zxbit@sina.com (X.Z.); dousl@hit.edu.cn (S.D.); yaoli@hit.edu.cn (Y.L.)

Abstract: A metal layer with high reflectance is widely used as the bottom mirror of smart radiation devices. Reduced solar absorption and enhanced emittance tunability are required for smart radiation devices applied in aerospace. Thus, reducing the absorption in the metal is also necessary. Here, Al films have been prepared by direct current magnetron sputtering on the fused silica substrate. The structure, morphology, and optical properties of the films have been analyzed at various deposition temperatures and deposition times. The spectrum absorption tends to increase with the increase of surface roughness due to the agglomeration and size increase of Al particles, which has been further demonstrated by the simulated results. The optimized Al film exhibits small solar absorption of 0.14 and low emittance of 0.02, which benefits the application for smart radiation devices and solar reflectors.

Keywords: Al film; solar absorption; thermal emittance; magnetron sputtering; deposition condition

Citation: Gu, J.; Zhao, X.; Ren, F.; Wei, H.; Liang, S.; Geng, C.; Guan, H.; Zhang, X.; Dou, S.; Li, Y. Investigation on Solar Absorption and Thermal Emittance of Al Films Deposited by Magnetron Sputtering. *Coatings* **2022**, *12*, 17. https://doi.org/10.3390/coatings12010017

Academic Editor: Christian Mitterer

Received: 2 December 2021
Accepted: 21 December 2021
Published: 23 December 2021

1. Introduction

The smart radiation device (SRD) is a promising technology for the thermal radiation regulation of spacecraft and satellites since they constitute the physical interface between the thermal management system and the space environment [1–3]. At the moment, the most promising SRD configuration consists of a bottom mirror, followed by a dielectric resonant cavity, and an active VO_2 film, which could dynamically regulate its radiation in response to the temperature [4]. An ideal dynamic SRD should have both a high infrared (IR) emittance tunability to achieve heat dissipation and preservation, and a low solar absorption to reflect the solar radiation [3,4].

As an important part of the SRD, the choice of the metal layer with high reflectance in the solar spectrum range and IR range is important [5,6]. Especially, to reduce the solar absorption of SRD, it is necessary to select the metal layer with low solar absorption. In addition, the emittance performance of the VO_2 strongly depends on the IR properties of the substrate, the high IR infrared reflectance can be conducive to obtaining large emittance tunability [7,8]. The aluminum (Al) film is widely used as the highly reflective broadband mirror for its low costs, easy preparation, and high intrinsic reflectivity from the far-ultraviolet to far-infrared [3,9]. Paul et al. prepared the highly reflective and adhesive Al thin films on Si wafers with the seed layers by direct current magnetron sputtering (DCMS) method, and demonstrated that the introduction of the seed layer could enhance reflectance in a broad spectral range and reduce long-term degradation [5]. Ning et al. investigated the thermal emittance of Al films in the solar selective absorbing coating, and the lowest thermal emittance for the Al film with the optimal thickness of 78 nm was obtained [10].

However, the influence of deposition temperature on the Al optical properties is not studied. In addition, the effect of deposition conditions on the solar absorption of the Al film has not been reported in the current reports.

Al film growth mode and quality highly affect the optical response of the film, and hence its optical properties. In this work, Al films were deposited on the fused silica by direct current magnetron sputtering. The effects of the deposition temperature, thickness, and surface roughness on the solar absorption and IR emittance of the Al films have been investigated. Furthermore, the effect of the surface particles on spectral performance was analyzed by theoretical simulation.

2. Materials and Methods

2.1. Sample Preparation

The fabrication process of the Al films is illustrated in Figure 1. Firstly, the chamber was initially evacuated to 2.1 $\times$ 10^{-4} Pa, and high purity argon (99.99%) was introduced during deposition. Then, the Al films were deposited by the DCMS method (MS650C, KeYou, Shenyang, China) from Al target (99.999%) onto 1 mm-thick fused silica substrate, which was dried after washing for 15 min both in acetone and ethyl alcohol using an ultrasonic cleaner to remove impurities on the substrate surface. The applied DCMS power was 100 W and the work pressure was kept at 0.9 Pa. The deposition temperature and time were adjusted to optimize the crystallinity and thickness of the Al films. The detailed parameters of the sputtering process were listed in Table 1.

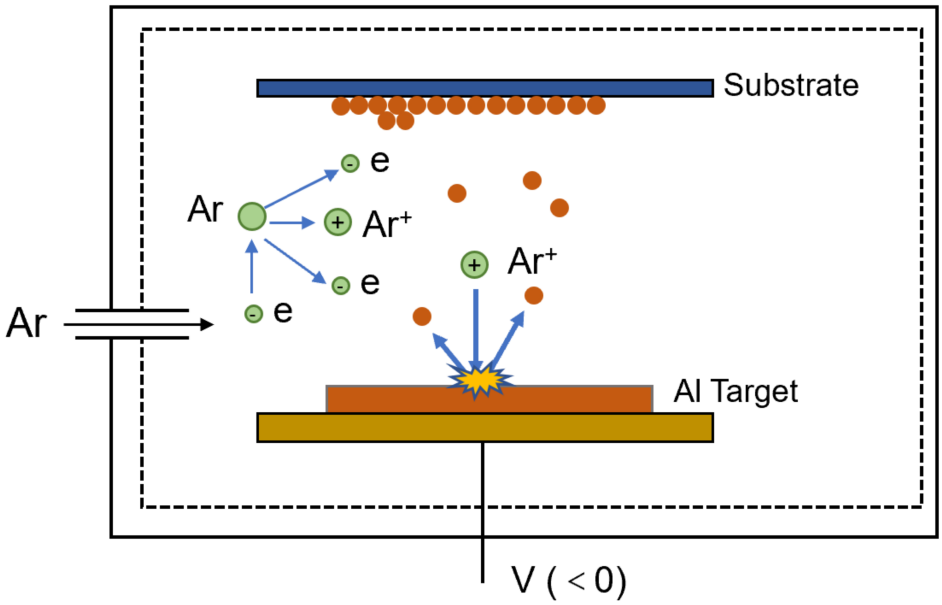

Figure 1. Schematic diagram of the Al film prepared by magnetron sputtering.

Table 1. Detail deposition parameters of the Al films.

Sample Number	#1	#2	#3	#4	#5	#6	#7	#8	#9
Deposition temperature/°C	RT	100	200	300	400	100	100	100	100
Deposition time/min	10	10	10	10	10	5	15	20	25

2.2. Characterization

Crystalline structures of the Al films were determined by X-ray diffraction (XRD, PANalytical, Almelo, The Netherlands) using Cu Kα radiation (λ = 0.15406 nm) at an X-ray grazing angle of 5°. Surface and cross-section morphologies of films were analyzed using a field emission scanning electron microscope (SEM, SUPRA 55 SAPPHIRE, ZEISS,

Oberkochen, Germany). Further, the surface roughness of the sample was evaluated from a randomly selected square area of 5 × 5 μm^2 by atomic force microscopy (AFM, Dimension Icon, Bruker, Karlsruhe, Germany) measurement.

For optical properties measurement, the reflectance spectra in the wavelength range of 0.25–2.5 μm and 2.5–25 μm were measured using a UV-VIS-NIR spectrophotometer (Lambda-950, Perkin Elmer, Waltham, MS, USA) and an FT-IR spectrometer (Vertex 70, Bruker, Karlsruhe, Germany) with an A562 integrating sphere, respectively. According to Kirchhoff's law, the spectral emittance and spectral absorptance of a body are equal at thermal equilibrium conditions. For an opaque material without transmission, the spectral emittance (ε) can be equal to the absorption (α). Then the emittance, as the averaging emittance, can be calculated by integrating the spectral emittance with the theoretical blackbody spectrum at the operating temperature according to the Equations (1) and (2) [1–3]:

$$B(\lambda,\ T) = \frac{2\pi hc_1^2}{\lambda^5} \cdot \frac{1}{e^{(\frac{hc_2}{\lambda kT})} - 1} \tag{1}$$

$$\varepsilon = \frac{\int_{\lambda_{min}}^{\lambda_{max}} (1 - R(\lambda)) \cdot B(\lambda, T) d\lambda}{\int_{\lambda_{min}}^{\lambda_{max}} B(\lambda,\ T) d\lambda} \tag{2}$$

where B (λ,T) is the blackbody radiation at temperature T.

Similar to emittance, the solar absorption is the average absorption weighted by the solar irradiance distribution using Equation (3), where $I_{AM1.0}$ is the spectral solar irradiance in the space [1].

$$\alpha = \frac{\int_{\lambda_{min}}^{\lambda_{max}} (1 - R(\lambda)) \cdot I_{AM1.0}(\lambda) d\lambda}{\int_{\lambda_{min}}^{\lambda_{max}} I_{AM1.0}(\lambda) d\lambda} \tag{3}$$

3. Results and Discussion

3.1. Crystal Structure of the Al Films

The thin film was characterized by grazing incidence XRD in order to obtain Al characteristic diffraction peaks. As shown in Figure 2, the 38.5° peak corresponds to (111) crystal planes of the Al films (JCPDS: 99-0005). As the lowest energy plane, (111) plane in growing films easily aligns parallel to the substrate [11]. In the partially enlarged view in Figure 2, the intensity of the (111) plane is very low at the deposition temperature of the RT. The intensity of the diffraction peak of (111) enhances when the deposition temperature is above 100 °C. However, the change of diffraction peak is unobvious with increasing temperature from 100 to 400 °C. It is mainly due to the short deposition time, which leads to the thin thickness.

3.2. Morphology of the Al Films

The surface morphologies of the Al films with the same deposition time (10 min) at different deposition temperatures are shown in Figure 3. The Al film deposited at RT is smooth with the small particles (Figure 3a), however, some cracks are observed due to the poor adhesion to the substrate. As the temperature further increases, the particle sizes increase obviously, and the particles gradually agglomerate (Figure 3b,c). When the deposition temperature reaches 300 °C, the films have formed an open microstructure with big islands and deep voids (Figure 3d,e), which can be attributed to the conversation of energy [12–15]. To reduce the total surface energy, the smaller grains with higher surface energy tend to detach and diffuse to the larger grains in the matrix [9,16]. The structure is further observed from the cross-sectional morphology. As the temperature increases from RT to 200 °C, the thickness of the films decreases from 190 nm to 130 nm, due to easily occurring migration and rearrangement of the sputtering particles at higher substrate temperature [17,18]. Then, it can be observed the hill-like structure at the temperature of 300 °C and 400 °C, therefore the average thickness increases. Similarly, the particle size

of the Al films gradually becomes larger with the deposition time increasing, and larger agglomerate particles appear at the deposition time of 25 min (Supplementary Materials, Figure S1). The thickness of the Al films appears to increase first from 100 nm to 180 nm, and then decrease to 160 nm.

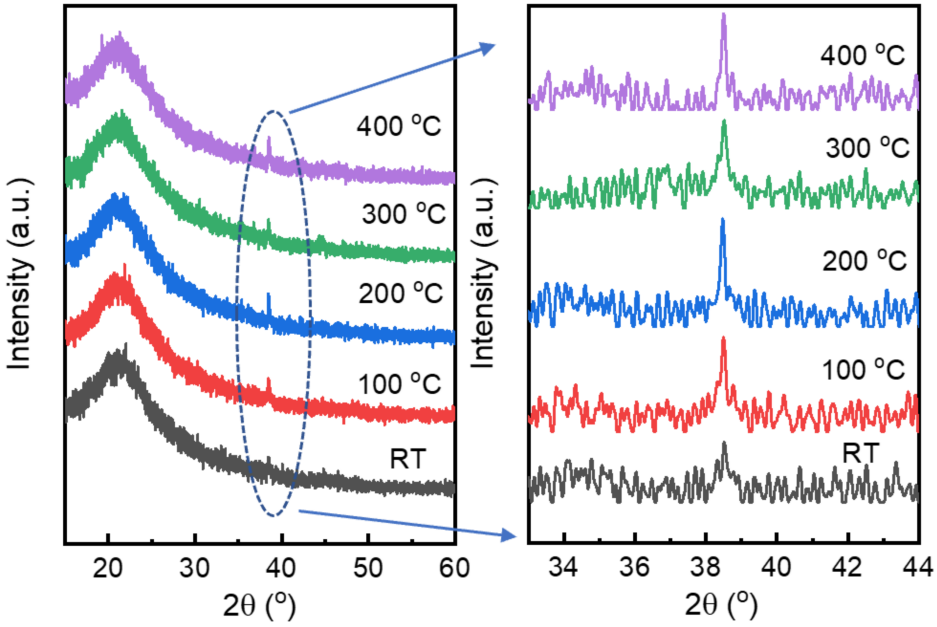

Figure 2. XRD pattern of the Al film at different deposition temperatures.

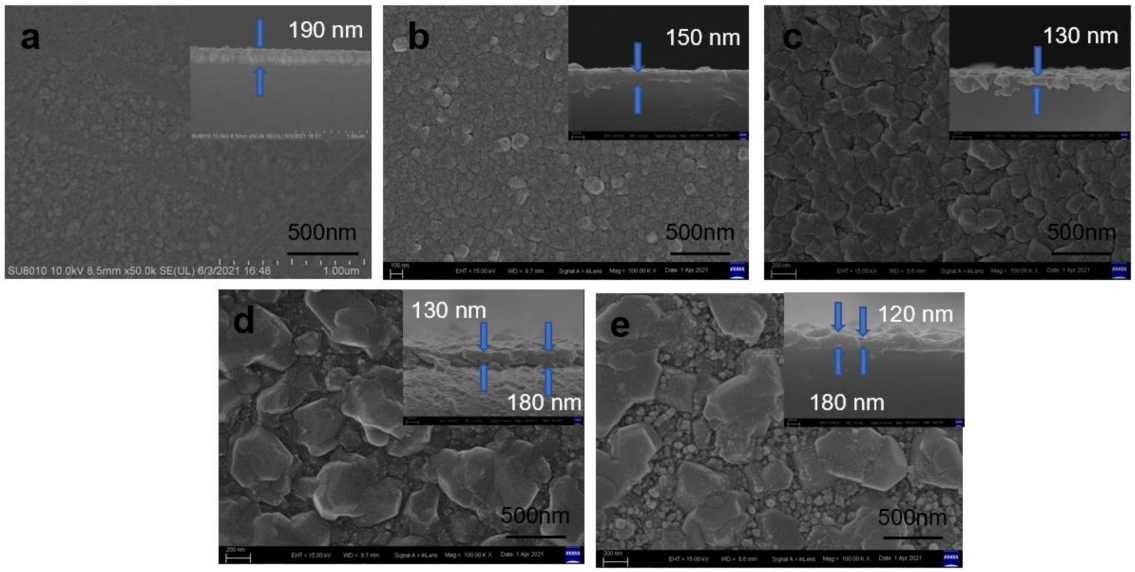

Figure 3. The morphologies of Al films at different deposition temperature: (**a**) RT, (**b**) 100 °C, (**c**) 200 °C, (**d**) 300 °C, (**e**) 400 °C. (The insets are the corresponding cross-sectional images).

The evolution of the surface morphology with the deposition temperature was analyzed by AFM measurements performed on 5 μm × 5 μm sample areas. As shown in Figure 4, the needle-like structure on the surface of the films is observed at low deposition temperatures. As the deposition temperature further increases, the Al film flows laterally to fill the surface pores leading to the formation of interconnected pits and valleys, and then forms the mountain-like structure (Figure 4d,e) [19]. The nanoparticles range from ~11 to ~180 nm in height and range from ~100 to ~900 nm in width (Figure S2), when the deposition temperature increases from RT to 400 °C. The increase of surface roughness

with the deposition temperature is evident, and the root means square roughness (Rq) increases obviously from 6.2 nm to 61.3 nm as the deposition temperature increase from RT to 400 °C. The result agrees with the analysis from the SEM images. About the influence of the deposition time on the morphological characteristics, it can be noted that Rq of the Al films also gradually becomes larger from 4.4 nm to 29.8 nm (Figure S3), and the nanoparticles range from ~14 to ~53 nm in height and range from 140 to 340 nm in width (Figure S4), as the deposition time increases from 5 min to 25 min. The details of surface roughness are listed in Table S1.

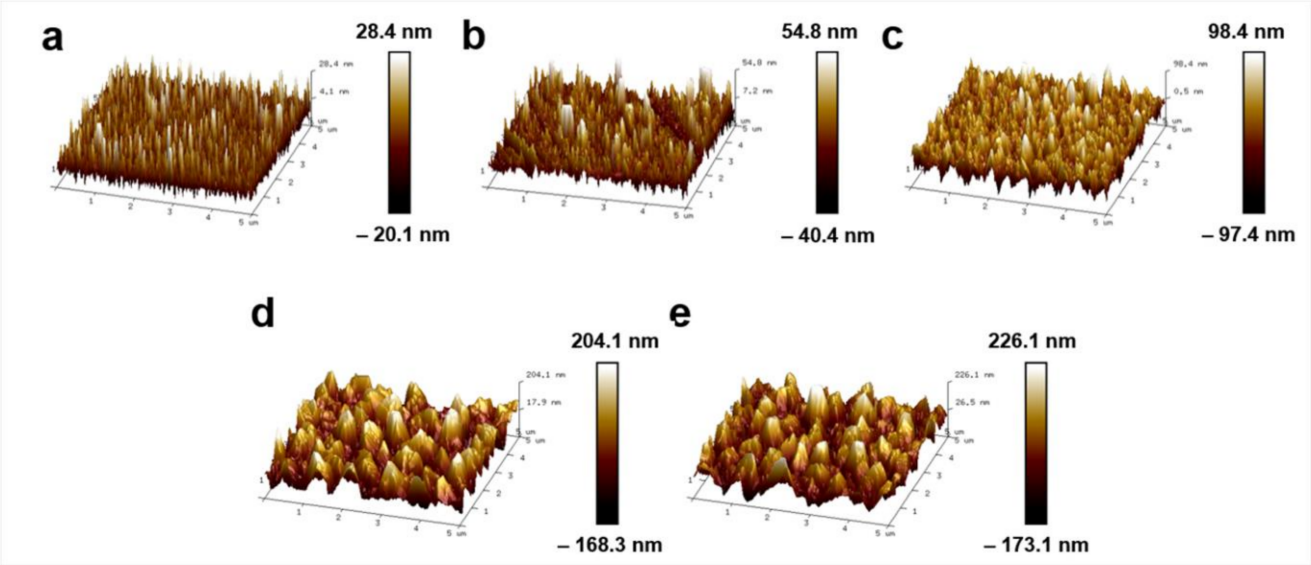

Figure 4. The AFM images of the Al films with different deposition time: (**a**) RT, (**b**) 100 °C, (**c**) 200 °C, (**d**) 300 °C, (**e**) 400 °C.

3.3. Reflectance Spectrum of the Al Films

3.3.1. Effect of Deposition Temperature on Reflectance Spectrum

The reflectance of Al films deposited at different temperatures is shown in Figure 5a,b. An obvious absorption peak appears at 840–860 nm and is slightly red-shifted accompanied by the widened bandwidth and the strengthened intensity (Figure 5a). According to the previous reports, the absorption peak at 800 nm is related to the interband transition due to the free electron-like behavior of the Al [14,20]. In addition, the reflectance of the Al films decreases in the wavelength of 0.25–2.5 μm as the deposition temperature increases. The variations of the spectra of the samples can attribute to the Al surface morphology. At low temperatures, the surface of the Al film consists of tiny particles with needle-like structure and the surface roughness is small. As the temperature reaches 200 °C, the hill-like structure is formed. With the deposition temperature continually increasing, the surface particles further aggregate. Therefore, larger particles with the size of hundreds of nanometers have formed and the film roughness has enhanced, resulting in the volume for both light–matter interactions and near-field coupling between neighboring nano-particles increases, which could strengthen and broaden the absorption, respectively [11,21,22]. Besides, it is easier to achieve impedance matching and reduce reflection due to the increased size of the Al particles [14]. Thus, the reflectance of the Al films decreased, and the absorption increased. The solar absorption of the Al films has increased from 0.09 to 0.44 with the deposition temperature increasing (Table S2). For the IR reflectance at 2.5–25 μm, the size of the Al particles is less than the mid-far infrared wavelength, and the difference of the Al film thickness is little. Therefore, all the samples show high IR reflectance (Figure 5b).

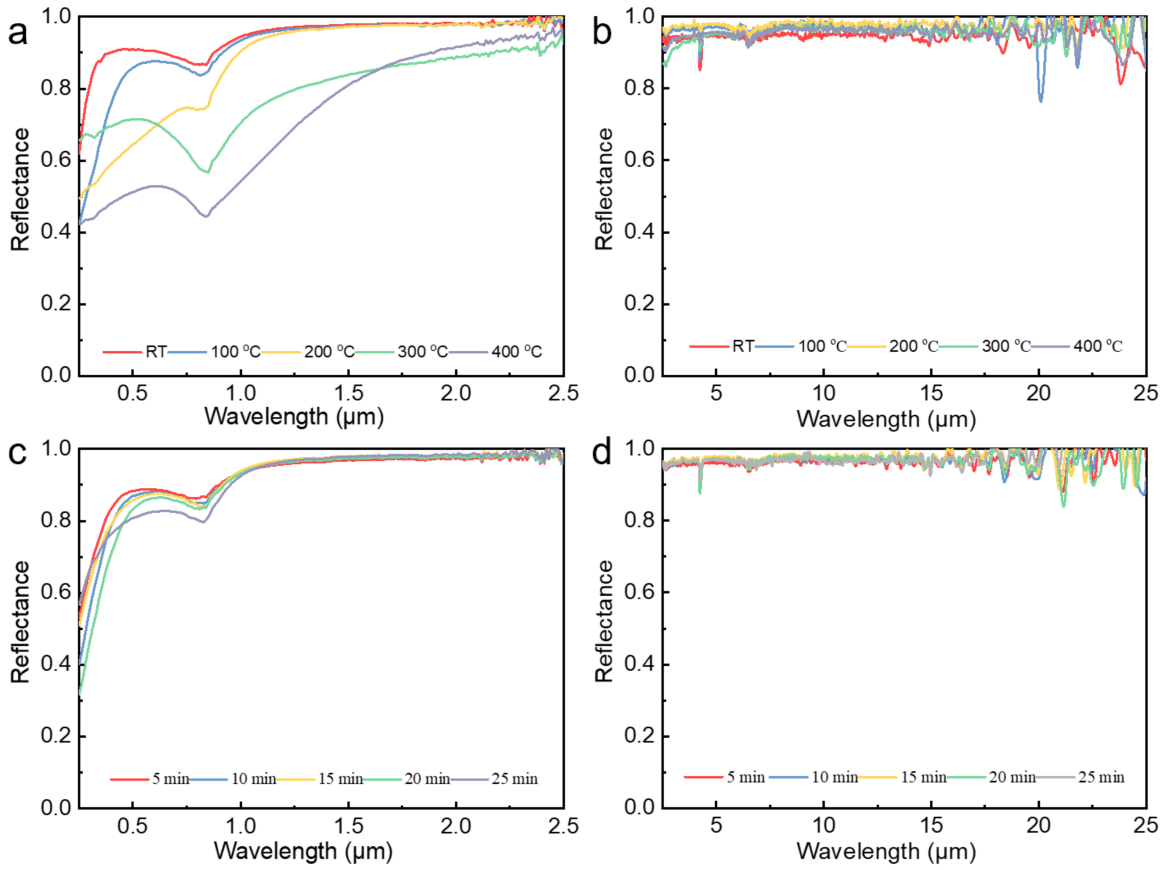

Figure 5. (**a**) UV-VIS-IR reflectance spectra and (**b**) NIR/MIR-IR reflectance spectra of the Al films at different deposition temperatures. (**c**) UV-VIS-IR reflectance spectra and (**d**) NIR/MIR-IR reflectance spectra of the Al films at different deposition time.

3.3.2. Effect of Deposition Time on Reflectance Spectrum

The effect of the deposition time on the reflectance spectra was studied as shown in Figure 5c,d. The spectrum reflectance of the Al films at 0.25–1.25 μm slightly decreases with the increase of the deposition time. The small difference exists in Al film thickness, while the size of the Al particles increases obviously, and surface roughness is enhanced, which contributes to the decrease of the Al film reflectance and the increase of the Al film absorption in the visible band (Figure 5c) [11,23,24]. In addition, the Al films show high reflectance at 1.25–25 μm due to the little difference in Al film thickness (Figure 5c,d). The optimum deposition time is around 15 min, and the solar absorption and IR emittance are 0.14 and 0.02, respectively.

3.3.3. Effect of Particle Size on Reflectance Spectrum

In order to further illustrate the effect of the particle size on the absorption at 0.25–2.5 μm, the UV-VIS-IR reflectance spectra of the Al films were simulated by finite-difference time domain (FDTD). The dielectric constant of the Al was from the database parameter of CRC. According to the actual surface morphology, the Trunc ellipse cone structure was selected as the basic unit, and the distribution of the particles is periodic (Figure 6a). In addition, w was the diameter of the particle, and h represented the height of the particle. As shown in the cross-sectional morphology (Figure 3 and Figure S1), Al particles existed on the surface of the Al film with a certain thickness. Therefore, an Al film with a thickness of 100 nm was set as an intermediate layer between the surface particle structure and the substrate in the simulation.

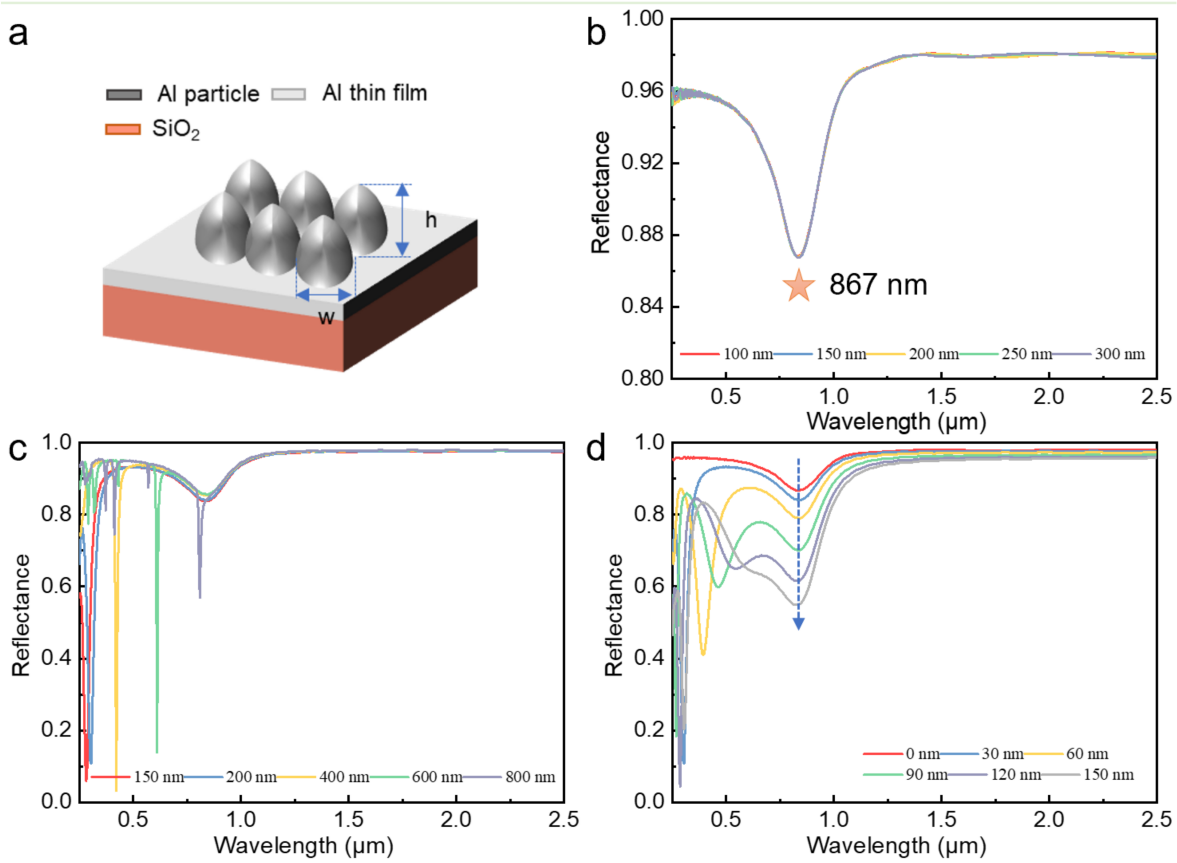

Figure 6. (**a**) Schematic representation of the Al films with nano-particles on the surface. (**b**) The simulated reflectance spectra of the planar Al films with no nano-particles. The simulated reflectance spectra of the Al films with the nano-particles: (**c**) particle height is 30 nm, width is from 150 nm to 800 nm, (**d**) particle height is from 30 nm to 150 nm, width is 200 nm.

The simulated reflectance spectrum of the planar Al films with no nano-particles is shown in Figure 6a. As shown in Figure 6b, the typical absorption peak at 867 nm is also observed due to the interband transition of the Al. However, the reflectance of the Al planar films has little change with the increase of the Al thickness. Figure 6c shows the reflectance for the Al nanoparticle height h of 30 nm, with width w varying from 150 nm to 800 nm, which is set according to the actual particle width in Figures S2 and S4. Sharper absorption peaks appear in the reflectance spectra due to the surface plasmon resonance by the Al particles. According to the Drude dispersion theory, the local surface plasmon resonance peaks of metal nanoparticles have a redshift effect as the diameter of the particles increases [25,26]. As the width of the Al particles increases, the absorption peak is redshifted and the intensity decreases. However, the width of the Al particles has little influence on the overall reflectance spectra, thus the reflectance of all the samples has little difference.

In Figure 6d, the plasmon resonance absorption is observed in 0.25–0.4 μm for the Al particles with a width of 200 nm. As reported, the forward Trunc ellipse cone structure is easy to achieve impedance matching and reduce reflection, and the higher the height, the more obvious the anti-reflection effect [27]. The reflectance has decreased obviously at 0.25–1.25 μm as the height increases from 30 nm to 150 nm, which is similar to the experimental results and has proved the influence of particle height on reflectance spectrum in theory. By contrast, the actual solar absorption of the Al films is larger due to the uneven particle size and disordered distribution on the surface of the prepared Al films.

4. Conclusions

The Al films were successfully fabricated on the fused silica substrate by DCMS. With the increase of the deposition temperature and time, the Al particles will grow and coarsen, resulting in the increase of surface roughness. Therefore, the reflectance of the Al films decreases obviously, and then the solar absorption increases. Furthermore, the simulation results by FDTD have further confirmed that the decrease in the height of the particle on the Al surface could reduce the solar absorption of the Al film. Besides, all the samples show high IR reflectance in the 2.5–25 μm. For the practical application, it is an effective way to reduce solar absorption of the Al films by decreasing the deposition temperature and time, which could reduce the particle size and surface roughness. Based on the optimized condition with the deposition temperature of 100 °C and deposition time of 10 min, the Al film exhibits small solar absorption of 0.14 and low emittance of 0.02, which is conducive to its application in smart radiation devices and solar reflectors.

Supplementary Materials: The following supporting information can be downloaded at: https://www.mdpi.com/article/10.3390/coatings12010017/s1, Figure S1: The surface micro-structure of the Al films with different deposition time: (a) 5 min, (b) 10 min, (c) 15 min, (d) 20 min, (e) 25 min. (The insets are the corresponding cross-sectional images). Figure S2: AFM image of Al films and height profiles in the directions of i and ii (guided by white lines). (a) Deposition temperature at RT, (b) Deposition temperature at 400 °C. Figure S3: The AFM images of the Al films with different deposition time: (a) 5 min, (b) 10 min, (c) 15 min, (d) 20 min, (e) 25 min. Figure S4: AFM image of Al films and height profiles in the directions of i and ii (guided by white lines). (a) Deposition time of 5 min, (b) Deposition time of 25 min. Table S1: Surface roughness of the Al films with different deposition temperatures and deposition time. Table S2: Solar absorption and infrared emittance of the Al films prepared under different deposition conditions.

Author Contributions: J.G., carried out the tests and wrote the manuscript, X.Z. (Xin Zhao), F.R., H.W., S.L., C.G. and H.G. performed the analysis of the results and assisted in the test, X.Z. (Xin Zhao), Y.L., X.Z. (Xiang Zhang) and S.D. contributed to the concept and modified the manuscript. All authors have read and agreed to the published version of the manuscript.

Funding: This research received no external funding.

Institutional Review Board Statement: Not applicable.

Informed Consent Statement: Not applicable.

Data Availability Statement: The data presented in this study are available on request from the corresponding author.

Conflicts of Interest: The authors declare no conflict of interest.

References

1. Sun, K.; Riedel, C.A.; Urbani, A.; Simeoni, M.; Mengali, S.; Zalkovskij, M.; Bilenberg, B.; Degroot, C.H.; Muskens, O. VO_2 Thermochromic metamaterial-based smart optical solar reflector. *ACS Photonics* **2018**, *5*, 2280–2286. [CrossRef]
2. Wei, H.; Gu, J.X.; Ren, F.F.; Zhang, L.P.; Xu, G.P.; Wang, B.; Song, S.S.; Zhao, J.P.; Dou, S.L.; Li, Y. Smart materials for dynamic thermal radiation regulation. *Small* **2021**, *17*, 2100446. [CrossRef] [PubMed]
3. Sun, K.; Riedel, C.A.; Wang, Y.D.; Urbani, A.; Simeoni, M.; Mengali, S.; Zalkovskij, M.; Bilenberg, B.; Groot, C.H.; Muskens, O.L. Metasurface optical solar reflectors using AZO transparent conducting oxides for radiative cooling of spacecraft. *ACS Photonics* **2018**, *5*, 495–501. [CrossRef]
4. Beaini, R.; Baloukas, B.; Loquai, S.; Klemberg-Sapieha, J.E.; Martinu, L. Thermochromic VO_2-based smart radiator devices with ultralow refractive index cavities for increased performance. *Sol. Energy Mater. Sol. Cells* **2020**, *205*, 110260. [CrossRef]
5. Taylor, S.; Yang, Y.; Wang, L.P. Vanadium dioxide based Fabry-Perot emitter for dynamic radiative cooling applications. *J. Quant. Spectrosc. Radiat. Trans.* **2017**, *197*, 76–83. [CrossRef]
6. Kim, H.; Cheung, K.; Auyeung, R.C.Y.; Wilson, D.E.; Charipar, K.M.; Piqué, A.; Charipar, N.A. VO_2-based switchable radiator for spacecraft thermal control. *Sci. Rep.* **2019**, *9*, 11329. [CrossRef] [PubMed]
7. Benkahoul, M.; Chaker, M.; Margot, J.; Haddad, E.; Kruzelecky, R.; Wong, B.; Jamroz, W.; Poinas, P. Thermochromic VO_2 film deposited on Al with tunable thermal emissivity for space applications. *Sol. Energy Mater. Sol. Cells* **2011**, *95*, 3504–3508. [CrossRef]

8. Du, Z.Y.; Li, M.; Xu, S.C.; Li, K.B.; Zou, F.X.; Zhang, R.R.; Li, G.H. VO_2-based intelligent thermal control coating for spacecraft by regulating infrared emittance. *J. Alloys Compd.* **2021**, *895*, 162679. [CrossRef]
9. Schmitt, P.; Stempfhuber, S.; Felda, N.; Szeghalmi, A.V.; Kaiser, N.; Tünnermann, A.; Schwinde, S. Influence of seed layers on the reflectance of sputtered aluminum thin films. *Opt. Express.* **2021**, *29*, 19472. [CrossRef]
10. Ning, Y.P.; Wang, W.W.; Sun, Y.; Wu, Y.X.; Liu, Y.F.; Man, H.L.; Wang, C.; Zhang, Y.; Zhao, S.X.; Tomasella, E.; et al. Investigation on low thermal emittance of Al films deposited by magnetron sputtering. *Infrared Phys. Technol.* **2016**, *75*, 133–138. [CrossRef]
11. Xu, K.; Hao, L.; Du, M.; Mi, J.; Yu, Q.H.; Li, S.; Wang, J.N.; Li, S.J. Thermal emittance of Ag films deposited by magnetron sputtering. *Vacuum* **2020**, *174*, 109200. [CrossRef]
12. Semaltianos, N.G. Thermally evaporated aluminium thin films. *Appl. Surf. Sci.* **2001**, *183*, 223–229. [CrossRef]
13. Michely, T.; Krug, J. *Islands Mounds and Atoms*; Springer Science & Business Media: New York, NY, USA, 2004.
14. Ma, S.B.; Liu, Q.; Qian, X.C.; Hong, R.J.; Tao, C.X. Controllability study of surface plasmon resonance spectra of aluminium nanoparticles. *Acta Optica Sin.* **2017**, *37*, 0931001.
15. Rincón-Llorente, G.; Heras, I.; Rincón-Llorente, E.; Schumann, E.; Krause, M.; Escobar-Galindo, R. On the effect of thin film growth mechanisms on the specular reflectance of aluminium thin films deposited via filtered cathodic vacuum Arc. *Coatings* **2018**, *8*, 321. [CrossRef]
16. Simrick, N.L.; Kilner, J.A.; Atkinson, A. Thermal stability of silver thin films on zirconia substrates. *Thin Solid Films* **2012**, *520*, 2855–2867. [CrossRef]
17. Gu, J.X.; Wei, H.; Ren, F.F.; Fan, Q.P.; Xu, G.P.; Chen, X.; Song, S.S.; Dou, S.L.; Zhao, J.P.; Li, Y. Fabrication and performances of double-sided HfO_2 anti-reflection films with ultra-high infrared transmittance. *J. Alloys Compd.* **2021**, *858*, 158337. [CrossRef]
18. Wang, Z.; Hui, Y.X.; He, A.F. Effect of argon oxygen ratio on the properties of HfO_2 thin films prepared by magnetron supttering at room temperature. *J. Xian Technol. Univ.* **2016**, *36*, 87–93.
19. Mwema, F.M.; Akinlabi, E.T.; Oladijo, O.P. Micromorphology of sputtered aluminum thin films: A fractal analysis. *Mater. Today Proc.* **2019**, *18*, 2430–2439. [CrossRef]
20. Yu, H. Controlled-Synthesis, optical properties and biological applications of aluminum nanoparticles. *JiLin Univ.* **2020**, *1*, 1–2.
21. Mandal, J.; Wang, D.; Overvig, A.C.; Shi, N.N.; Paley, D.; Zangiabadi, A.; Cheng, Q.; Barmak, K.; Yu, N.F.; Yang, Y. Scalable, "Dip-and-Dry" Fabrication of a Wide-Angle Plasmonic Selective Absorber for High-Efficiency Solar–Thermal Energy Conversion. *Adv. Mater.* **2017**, *29*, 1702156. [CrossRef]
22. Boer, K. *Advances in Solar Energy*; Plenum Press: New York, NY, USA, 1986; Volume 3.
23. Cao, L.Q.; He, Z.; Sha, W.; Chen, R.S. Influence of geometry of metallic nanoparticles on absorption of thin-film organic solar cells: A critical examination. *IEEE Access* **2020**, *99*, 1. [CrossRef]
24. Kim, W.M.; Ku, D.Y.; Lee, K.S.; Cheong, B. Effect of oxygen content and deposition temperature on the characteristics of thin silver films deposited by magnetron sputtering. *Appl. Surf. Sci.* **2010**, *257*, 1331–1336. [CrossRef]
25. Kaune, G.; Metwalli, E.; Meier, R.; Körstgens, V.; Schlage, K.; Couet, S.; Röhlsberger, R.; Roth, S.V.; Müller-Buschbaum, P. Growth and morphology of sputtered aluminum thin films on P3HT surfaces. *ACS Appl. Mater. Interfaces* **2011**, *3*, 1055–1062. [CrossRef]
26. Tong, L.M.; Xu, H.X. Surface plasmons-mechanisms, application and perspectives. *Physics* **2012**, *41*, 582–588.
27. Vu, T.C.; Cao, X.; Hu, H.B. A universal robust bottom-up approach to engineer Greta-oto-inspired anti-reflective structure. *Cell Rep. Phys. Sci.* **2021**, *2*, 100479. [CrossRef]